

# Prompt and afterglow early X-ray phases in the comoving frame. Evidence for Universal properties?

*G. Chincarini<sup>1,2</sup>, A. Moretti<sup>2</sup>, P. Romano<sup>2</sup>, S. Covino<sup>2</sup>, G. Tagliaferri<sup>2</sup>, S. Campana<sup>2</sup>, M. Goad<sup>3</sup>, S. Kobayashi<sup>4</sup>, B. Zhang<sup>5</sup>, L. Angelini<sup>6</sup>, P. Banat<sup>2</sup>, S. Barthelmy<sup>6</sup>, A.P. Beardmore<sup>3</sup>, P.T. Boyd<sup>6</sup>, A. Breeveld<sup>7</sup>, D.N. Burrows<sup>4</sup>, M. Capalbi<sup>8</sup>, M.M. Chester<sup>4</sup>, G. Cusumano<sup>9</sup>, E.E. Fenimore<sup>10</sup>, N. Gehrels<sup>6</sup>, P. Giommi<sup>8</sup>, J.E. Hill<sup>6</sup>, D. Hinshaw<sup>6</sup>, S.T. Holland<sup>6,11</sup>, J.A. Kennea<sup>4</sup>, H.A. Krimm<sup>6</sup>, V. La Parola<sup>9</sup>, V. Mangano<sup>9</sup>, F.E. Marshall<sup>6</sup>, K.O. Mason<sup>7</sup>, J.A. Nousek<sup>4</sup>, P.T. O'Brien<sup>3</sup>, J.P. Osborne<sup>3</sup>, M. Perri<sup>8</sup>, P. Mészáros<sup>4</sup>, P.W.A. Roming<sup>4</sup>, T. Sakamoto<sup>6</sup>, P. Schady<sup>6</sup>, M. Still<sup>6</sup>, A.A. Wells<sup>3</sup>.*

<sup>1</sup> Università degli studi di Milano-Bicocca, Dipartimento di Fisica, Italy

<sup>2</sup> INAF -Osservatorio Astronomico di Brera, Italy

<sup>3</sup> Department of Physics and Astronomy, University of Leicester, Leicester, LE 1 7RH, UK

<sup>4</sup> Department of Astronomy and Astrophysics, Pennsylvania State University, USA

<sup>5</sup> Department of Physics, University of Nevada, Las Vegas, NV 89154-4002, USA

<sup>6</sup> NASA - Goddard Space Flight Centre, USA

<sup>7</sup> Mullard Space Science Laboratory, University College London, UK

<sup>8</sup> ASI Science Data Center, Italy

<sup>9</sup> INAF- Istituto di Astrofisica Spaziale e Fisica Cosmica Sezione di Palermo, Italy

<sup>10</sup> Los Alamos National Laboratory, New Mexico, USA

<sup>11</sup> Universities Space Research Association

## Abstract

We analyze the Swift XRT light curves and spectra of the gamma-ray bursts (GRBs) for which the redshift has been measured. The sample consists of seven GRBs. The soft X-ray light curves of all these GRBs are separated into at least two morphological classes: 1) those starting off with a very steep light curve decay and 2) those showing a rather mild initial decay. This initial decay is followed by a flattening and by a further steepening. During these transitions the soft X-ray spectrum of these GRBs remains constant within the observational errors (except for one case, GRB050319). For the first time we are able to exploit the early light curve of GRB afterglows in the comoving frame. Besides the temporal and spectral behavior we find that the energy of the afterglow emitted in the (rest frame) time interval 20-200 s and 1300-12600 s after the trigger correlates with the mean energy of the prompt emission, hinting at a close link between the two. Averaging over the bursts that have a rather well sampled light curve and starting immediately after the prompt phase, the energy emitted in the soft X-rays is about 3% of the energy emitted during the prompt phase, except for GRB050315, where the soft X-ray emission is as high as 14% of the prompt emission.

## 1. Introduction.

Following the discovery of GRB afterglows by BeppoSAX (Costa et al. 1997) and the subsequent development of theoretical models to explain these spectacular cosmic explosions (e.g. Mészáros and Rees 1997 and references therein), a clear picture of the GRB phenomenon has emerged. For a thorough review of the excellent early work in this field see the review papers by Piran (2004), Hurley, Sari and Djorgovski (2003), Zhang and Mészáros (2004).

The primary goal of the Swift Gamma-ray Burst Explorer (Gehrels et al. 2004) launched on Nov 20, 2004, was not only to detect a statistically significant sample of GRBs, but also to collect related data in the X-ray band (0.2-10 keV) and at optical wavelengths (1700 – 6500 Å) in the as yet little understood initial few tens of seconds after the trigger.

At the present time, Swift is collecting a large amount of new data, with seemingly every burst displaying its own peculiar characteristics. Indeed, with every new prompt XRT observation of a burst, new details are emerging (e.g. Burrows et al. 2005a; Campana et al. 2005a; Tagliaferri et al. 2005; Cusumano et al. 2005; Burrows et al. 2005b).

In an effort to determine how many GRB classes we are actually sampling, and to understand the physical reasons behind the observed differences, we here primarily follow an observational approach and look for common characteristics in their light curves. Here we report the results of a pilot study on a small, but statistically significant sample of GRBs for which we have both early observations in the XRT and a spectroscopic redshift for the optical transient. Choosing the sample in this fashion will enable us to disentangle intrinsic physical properties from those related to GRB distance. The present study will serve as the basis for the analysis of a larger sample for which more significant statistics will be possible.

## 2. The observations

The present sample includes all GRBs (seven) observed by Swift up to May 15 for which it has been possible to obtain a redshift from optical spectroscopy. Of these seven GRBs, six were discovered by the Burst Alert Telescope (BAT, Barthelmy et al. 2004) on board Swift and the other by HETE2. These seven objects are listed in Table 1.

Telescope (XRT) on board Swift (Burrows et al. 2005c). The XRT CCD has been designed to automatically switch between observing modes so that bright sources may be observed without any pile up effect (when two photons hit the same pixel during a CCD readout frame). For a thorough description of XRT observing modes and switch points see Hill et al. (2004). However, in the early stages of the mission some of the GRB afterglows interrupted ongoing XRT calibration observations of known sources. For these observations XRT was in manual state and hence on slewing to the burst position the normal sequence of observations were not performed. For the few GRBs affected in this way, the X-ray observations were usually performed in photon counting (PC) mode and for the brighter sources the XRT data are severely piled-up. This effect can be corrected by extracting light curves and spectra from an annular region around the source center (rather than a simple circular region), with a ‘hole’ the size of which is a function of the source brightness. The total flux is then recovered by using the PSF analytical model. As the afterglow decays the

**Table 1**

Burst	Redshift	T90	Fluence 15 – 350 keV erg cm <sup>-2</sup>	Refrences
GRB050126	1.29	25.8	$2.0 \cdot 10^{-6}$	1
GRB050315	1.949	50.4	$3.1 \cdot 10^{-6}$	2
GRB050318	1.44	9.1	$1.5 \cdot 10^{-6}$	3, 2
GRB050319	3.24	160.5 (&)	$1.7 \cdot 10^{-6}$	4,2
GRB050401	2.9	34.0	$1.5 \cdot 10^{-5}$	5
GRB050408	1.2357	/	/	6
GRB050505	4.27	62.0	$4.4 \cdot 10^{-6}$	7

(&) The BAT light curve shows two flares. The second with  $T_{90} = 23.5$  s, Fluence  $7.3 \cdot 10^{-7}$  erg cm<sup>-2</sup> and the first preceding it by 137 seconds, Fluence  $1.6 \cdot 10^{-6}$  erg cm<sup>-2</sup>. (T-90 is the time needed to accumulate from 5% to 95% of the counts in the 15-350 keV band).

REFERENCES: - (1) Campana et al. (2005b), Sato et al. (2005), Berger et al. (2005a); (2) Beadmore, et al. (2005), Parsons, et al. (2005), Kelson, et al. (2005); (3) Krimm, et al. (2005a), Berger, et al. (2005b); (4) Krimm, et al. (2005b), Fynbo, et al. (2005a); (5) Angelini, et al. (2005), Markwardt, et al. (2005), Fynbo, et al. (2005b); (6) Chincarini et al. (2005), Sakamoto et al. (2005), Prochaska, et al. (2005); (7) Hullinger, et al. (2005).

pile up effect diminishes and extraction from a circular region is then feasible. For the last four bursts discussed here the automatic mode switching was active and for three of them the observations started in window-timing (WT) mode (providing just 1D imaging) because of the high count rate. Cross calibration between modes ensures that the two modes (ie. PC and WT) do not introduce artificial variations in flux. In our analysis we extracted the X-ray spectra and light curves from a circular region of 30 pixels radius for PC mode, and a rectangular region of 40x20 pixels in WT mode, centered on the source position as determined from the Swift analysis task `xrtcentroid`. The extraction regions for the cases where pile-up is significant are detailed below where we discuss the single sources. At low count rates the XRT background (which is in any case very low due to the low Earth orbit of Swift) must also be taken into consideration. We evaluate the background over an annulus, avoiding detectable or known background sources, centered on the GRB position and delimited by 50 and 90 pixels (internal and external radius, respectively). In WT mode we used a 40x40 pixel region at a distance of 50 pixels from the source. The mode in which the various sources were observed is described below:

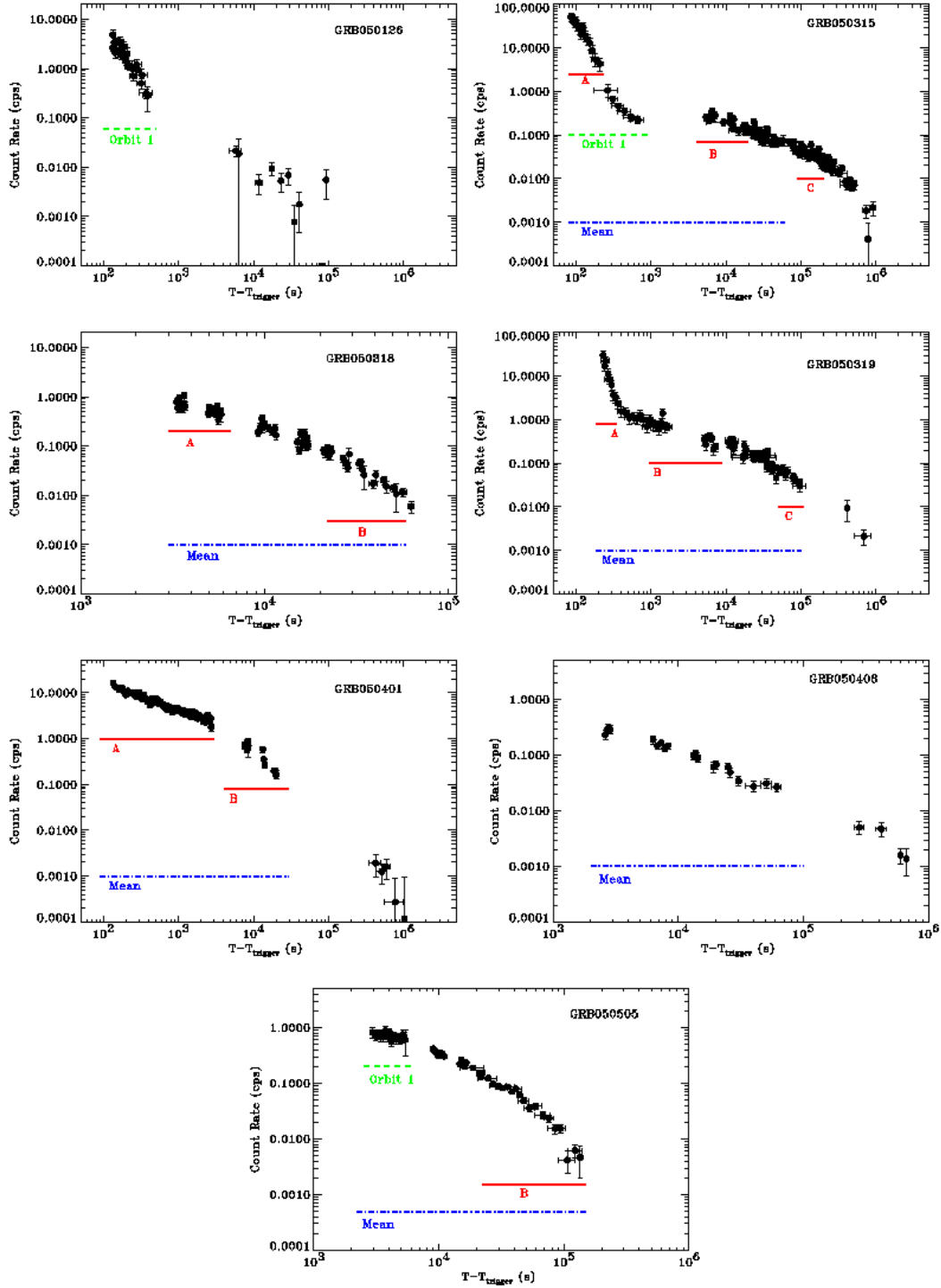


Figure 1. Light curves of the bursts discussed in this paper. For each light curve we have marked the time interval over which the spectra were reexecuted.

### GRB050126

Swift promptly slewed to the burst and XRT started observations 129 s after the BAT trigger. When the burst trigger occurred, XRT was operating in manual state in PC mode. Consequently the first set of data (300 s) is affected by pile-up. To account for pile-up we extracted an annular region of inner radius 3 pixels and outer radius 30 pixels. This region includes 50% of the Encircled Energy Fraction (EEF, Moretti et al. 2004). For more details on the analysis of this burst see Tagliaferri et al. (2005) and Goad et al. (2005).

### GRB050315

The observatory executed an automated slew to the BAT position and the XRT began taking data 83 s after the burst. The XRT was in a manual state and performed observations in PC mode only. As in the previous case, the first orbit data are severely piled up. This forced us to consider only the data from an annulus with an internal radius of 7 pixels; this provides only 20% of the EEF.

### GRB050318

When BAT detected GRB 050318 the position was within the Swift Earth horizon constraint. Thus, an automatic slew could not be performed until some 55 min after the BAT trigger. After the slew XRT began taking data in PC mode as the afterglow was still piled up; therefore the extracted events in an annular region of radii 3 and 25.

### GRB050319

For this burst the spacecraft was in automatic mode and executed an immediate slew arriving on target 87 s after the BAT trigger. Due to the brightness of the source, XRT began taking data in WT mode. During the first orbit, the GRB position fell near the edge of the WT mode window. This forced us to correct the WT data flux by the fraction of the EEF left out of the window. After the first 50 s XRT switched to PC mode, and up to the end of the 4<sup>th</sup> orbit data were affected by pile-up. The afterglow then faded and the following observations were taken in PC mode without any pile up (details in Cusumano et al. 2005). In order to correct for pile-up we used an annulus of inner and outer radius of 6 and 30 pixels for the first 4 orbits. A re-analysis of the prompt light curve by the BAT team found that the GRB did not start at the BAT trigger time reported in GCN 3117, Krimm et al. (2005b), but 137 s earlier. BAT did not trigger at this time as it was slewing from one part of the sky to another. Luckily, a final bright peak occurred which triggered the BAT. Here we report our analysis assuming as initial time the start time of the first peak of the prompt emission (see Cusumano et al. 2005 for more details).

### GRB050401

The spacecraft executed an immediate slew and was on target 137 s after the trigger. XRT was in autostate and began taking data in WT mode. The source was well within the WT window. In subsequent orbits data were collected in PC mode, and the PC source extraction region was an annulus of radii 9 and 30 to account for piled up.

### GRB050408

This burst was detected by HETE2. Swift did not slew automatically to the burst position. Instead a ToO (Target of Opportunity) was necessary to re-point the Swift observatory to

the burst position. XRT started observing 42 min after the HETE2 trigger. The afterglow had already faded and observations were taken in PC mode.

#### GRB050505

As for GRB050318, when BAT was triggered by the GRB 050505, the spacecraft was within the Earth bright limb observing constraint and could not perform an immediate slew: the XRT observations started 47 minutes after the trigger. At this time the source was still piled up and the PC source extraction region was an annulus of radii 3 and 30 to account for piled up.

### 3. Data analysis

For each burst we extracted the X-ray light curve using the extraction regions discussed above. In order to arrive at a homogeneous set of light-curves we grouped the counts for each source in bins of at least 30 counts. A typical XRT observation of a GRB lasts between 5 to 8 days with about 10% of the time effectively dedicated to each burst (for the remainder of the time the satellite points either to other GRBs or to other sources). For each orbit ( $\sim 5800$  s) a burst is typically observed for about 1000s / GRB / orbit. This means that for later times, when the source counts are low, we must bin over several orbits to make secure source detections and to satisfy the required number of counts per bin. The light curves for all of the bursts in our sample are shown in Fig. 1. For each burst we take the origin of time as the BAT trigger time. These light curves show steep decays and slope changes, with count rates spanning 4-5 decades.

In order to convert the count-rate light curves to fluxes and then luminosities, we need to calculate the counts to flux conversion factors from the spectral analysis. For each GRB afterglow, the XRT spectra of the source and background were extracted in the same regions used to extract the light curves. We first extracted an average spectrum for each GRB. Ancillary response files were generated with the task *xrtmkarf* within FTOOLS v6.0, to account for the different extraction regions. Spectral redistribution matrices (RMF) were retrieved from the latest Swift Calibration Database) distribution (CALDB 20050405: <http://heasarc.gsfc.nasa.gov/docs/heasarc/caldb/swift/>).

The spectra were then re-binned with a minimum of 20 counts per energy bin to allow  $\chi^2$  fitting within XSPEC 11.3.2. We first performed a fit of the mean spectrum of each burst with an absorbed power law model leaving the column density ( $N_H$ ) as a free parameter. If in the best fit model,  $N_H$  was found to be consistent with zero, or below the Galactic value, we froze  $N_H$  at the Galactic value. The resultant fits are reported in Table 2. All errors are 90% confidence limits on one interesting parameter.

For each afterglow we also looked for temporal spectral variations concentrating in particular in variations across breaks in the light curves. Here the compromise was between selecting a region in time before and after the break large enough to have sufficient counts to produce a meaningful spectrum. The selected regions are marked for each spectrum in Figure 1 (pile up correction have been applied when needed). When statistics did not allow  $\chi^2$  minimization we did not re-bin the spectra and instead used the Cash-statistic. The results are reported in Table 2. As can be seen from the values reported in Table 2, the spectra are consistent with no variation within the errors. Thus, we conclude that during the

**Table 2**  
**XRT – Spectra 0.2 – 10 keV (1)**

	Energy Index	$N_H / 10^{22} \text{ cm}^{-2}$ (2)	$\chi^2 / \text{dof}$	Notes (3)
GRB050126	$1.26 \pm 0.22$	$0.0528 \text{ Gal}$	$1.06 / 8$	Mean Spectrum
GRB050315	$1.13 \pm 0.09$	$0.15 \pm 0.02$	$1.58 / 121$	Mean Spectrum
	$1.37^{+0.17}_{-0.16}$	$0.13 \pm 0.04$	$0.65 / 42$	Orbit 1
	$1.34^{+0.15}_{-0.14}$	$0.13^{+0.03}_{-0.02}$	$0.63 / 43$	A
	$0.93^{+0.16}_{-0.14}$	$0.15^{+0.04}_{-0.03}$	$1.39 / 41$	B
	$0.95^{+0.13}_{-0.12}$	$0.15 \pm 0.03$	$1.08 / 59$	C
GRB050318	$0.87 \pm 0.09$	$0.041^{+0.012}_{-0.010}$	$0.88 / 74$	Mean Spectrum
	$0.99^{+0.16}_{-0.14}$	$0.054^{+0.027}_{-0.018}$	$0.72 / 28$	A
	$1.24^{+0.30}_{-0.25}$	$0.076^{+0.038}_{-0.027}$	$0.99 / 15$	B
GRB050319	$0.94^{+0.09}_{-0.08}$	$0.027^{+0.009}_{-0.008}$	$0.90 / 125$	Mean Spectrum
	$1.94^{+0.13}_{-0.20}$	$0.0113 \text{ Gal}$	$281.56 / 526$	A (Cash Stat)
	$0.79^{+0.13}_{-0.11}$	$0.0113 \text{ Gal}$	$376.38 / 478$	B (Cash Stat)
	$0.62^{+0.17}_{-0.18}$	$0.0113 \text{ Gal}$	$1.33 / 10$	C
	$0.75^{+0.20}_{-0.14}$	$0.0113 \text{ Gal}$	$361.53 / 478$	C (Cash Stat)
GRB050401	$1.10 \pm 0.06$	$0.214^{+0.020}_{-0.019}$	$1.11 / 258$	Mean Spectrum
	$1.07 \pm 0.06$	$0.210^{+0.020}_{-0.019}$	$1.09 / 249$	A
	$1.09 \pm 0.06$	$0.212 \pm 0.200$	$1.06 / 245$	B
	$1.33^{+0.43}_{-0.36}$	$0.293^{+0.155}_{-0.129}$	$0.77 / 10$	C
GRB050408	$1.14^{+0.20}_{-0.18}$	$0.248^{+0.053}_{-0.046}$	$1.32 / 38$	Mean Spectrum
GRB050505	$0.95 \pm 0.06$	$0.067 \pm 0.08$	$1.06 / 174$	Mean Spectrum
	$0.98 \pm 0.13$	$0.075 \pm 0.022$	$0.89 / 38$	Orbit 1
	$0.91 \pm 0.09$	$0.062 \pm 0.013$	$1.11 / 72$	B

(1) Modeled with a power-law with photoelectric absorption

(2) Gal = Milky Way absorption

(3) The interval of time over which the spectrum has been measured is given in Figure 3. Cash Stat means that we used the cash statistics in the best fit procedure.

evolution of the soft X-ray decay light curve we do not see corresponding spectral evolution. The mean spectrum energy index  $\beta$  (where  $f_v \propto v^{-\beta}$ ), of the observed bursts is  $\langle \beta \rangle = 1.08 \pm 0.27$ . The scatter is larger than the typical measurement errors which implies there exists a physical dispersion of the Energy Index among bursts, albeit rather small. GRB050319 is an exception to this rule. In this case the spectrum is very soft soon after the burst (indeed it is the softest spectrum measured) and becomes significantly harder at later times. GRB050315 may indicate a similar variation at a very low significance level while GRB050318 might show an evolution in the opposite sense. Indeed as stated above there is some physical variation that we must uncover with more statistics.

For each GRB we also extracted a prompt BAT spectrum to compare it with the XRT spectrum from the steep decline phase. For all bursts the average BAT spectrum is well fitted with a single unabsorbed powerlaw. The fits have been carried out in the energy range 20 – 150 keV where we know, at the time of writing, the calibration to be best. In Table 3 we report the best fit spectral energy index  $\beta$ . Qualitatively there seem to be two classes of bursts, one class with a harder spectrum ( $\beta < 0.5$ ), and the other with a softer spectrum ( $\beta > 1$ ). By contrast, the mean XRT spectrum immediately following the burst (see Table 2) is always characterized by an energy index  $\beta \geq 1$ . The indication is that in 3 cases

**Table 3: BAT–XRT Energy**

GRB	Energy Index BAT spectra	E/10 <sup>50</sup> 15-350 keV erg	E/10 <sup>50</sup> XRT Range T1, T2 erg (1)	E/10 <sup>50</sup> XRT Range T3, T4 erg (2)	E/10 <sup>50</sup> XRT Obs Tot erg (3)	Range (Log sec) of XRT data (4)
050126	0.32 ± 0.18	177.1	0.59	0.44	1.25	1.77-4.1
050315	1.18 ± 0.11	815.9	3.88	28.3	117.4	1.46-5.49
050318	1.16 ± 0.13	193.8	/	4.49	4.92	3.13-4.41
050319	1.13 ± 0.28	2145.8	21.5	58.11	160.3	1.35-5.21
050401	0.13 ± 0.09	10720.7	43.5	126.6	327.7	1.54-5.42
050408	0.32 ± 0.18	/	/	6.5	22.7	3.07-5.47
050505	0.27 ± 0.15	7381.9	/	171.8	250.7	2.75-4.41

(1) T1 = 50 s, T2 = 200 s after the BAT trigger.

(2) T3 = 1300 s, T4 = 12600 s after the BAT trigger.

(3) Total Energy observed by XRT.

(4) Gaps during the observations are present.

we progress from a rather hard prompt emission to a softer afterglow, but it is not completely clear whether these characteristics are related to the morphology of the light curves. If the missing observations of GRB050318 soon after the prompt emission had been characterized by a rapid decline, then we can safely argue that light curve morphology does play a role. Within errors the energy index of the BAT spectra GRB050315, GRB050318, GRB050319 (Table 3 column 2, Mean =  $1.16 \pm 0.32$ ) is the same as the energy index of the XRT spectra ( $1.08 \pm 0.27$ ). This is an indication, to be tested by future observations however, that a rapid decline of the post prompt emission is characterized by a rather soft spectrum with an energy index that is similar for the hard and soft X rays. GRB050126 is a possible exception.

### 3.1 XRT light curve analysis

To assess whether there are common features in the X-ray light curves, we converted them from count rates to fluxes, using the conversion factors derived from the spectral analysis of the average spectrum for each burst. We then computed the luminosity in a  $H_0 = 70$  km/s/Mpc,  $\Omega_m = 0.3$ ,  $\Omega_\Lambda = 0.7$  universe. The light curves are presented in Figure 2. After correcting the temporal scale to the source rest frame using the spectroscopic redshifts, the XRT observations began about 20 to 30 seconds after the BAT trigger. In Figure 2 the squares mark the average BAT luminosity observed during the prompt phase. For each burst we only report the average prompt luminosity estimated over the  $T_{90}$  spectrum. This choice was made to avoid overcrowding of the plot (see however Figure 3 in which we plot the 4 GRBs for which we have XRT light curves immediately following the BAT observations).

In order to model the XRT light curves shown in Fig. 2, we employ three different methods. In the first method, we fit the light-curve with a powerlaw with either one or two breaks. For the former the analytic expression is:

$$F(t) = \frac{K}{(t/t_{break})^{\delta_1} + (t/t_{break})^{\delta_2}}$$

where  $\delta_1$  and  $\delta_2$  are the two different slopes. For the latter we adopt:

$$F(t) = A \left( \frac{t}{t_{br \text{ first}}} \right)^{-\delta_1} + \frac{K}{(t/t_{break})^{\delta_2} + (t/t_{break})^{\delta_3}}$$

These equations, however, imply at any time the superposition of two (in the first case) and three (in the second case) signals, so that the true value of the slopes is biased if the slopes evolve with time. In practice this is a reasonable approach and these values are reported for each object in the first row of Table 4. The second method we considered involved estimating the slope of the light curves within intervals away from the breaks in the light-curves. Therefore, we excluded the data close to the break times and the remaining parts of the curve were fit with power laws. Our result for this second approach are reported in the second row of Table 4. In the final method we estimated the slopes by deriving the tangent to the fitting curve at various points along the light-curve. The results for this fitting method are reported in the third row of each burst in Table 4.

**Table 4. Slopes and breaks of the light curves.**

	Temporal slope Index Phase 1	Break Log sec First (1)	Temporal slope index Phase 2	Break Log sec Second (1)	Temporal slope index Phase 3	Notes
GRB050126	$-3.40^{+0.94}_{-2.05}$	$2.11^{+1.7}_{-0.52}$	$-0.94 \pm 0.36$			
	$-2.68 \pm 0.18$	$2.44 \pm 0.83$	$-0.66 \pm 0.35$			
	$2.67 \pm 0.22$	$3.00 \pm 0.40$	$-0.56 \pm 0.05$			
GRB050315	$-4.02 \pm 0.27$	$2.04 \pm 0.13$	$-0.20 \pm 0.05$	$4.5 \pm 0.28$	$-1.65 \pm 0.18$	(2)
	$-3.25 \pm 0.19$	$2.16 \pm 0.19$	$-0.14 \pm 0.069$ $-0.67 \pm 0.11$	$3.45 \pm 1.26$ $4.97 \pm 1.46$	$-2.65 \pm 0.39$	
	$-3.28 \pm 0.89$	$2.45 \pm 0.48$	$0.14 \pm 0.26$ $-0.67 \pm 0.26$	$3.21 \pm 0.14$ $4.77 \pm 0.30$	$-2.47 \pm 0.55$	(3)
GRB050318			$-0.89^{+0.38}_{-0.19}$	$3.95 \pm 0.55$	$-2.63 \pm 0.50$	
			$-1.04 \pm 0.09$	$3.89 \pm 0.97$	$-2.41 \pm 0.21$	
			$-1.05 \pm 0.07$	$3.7 \pm 0.05$	$-2.38 \pm 0.28$	
GRB050319	$-7.64 \pm 3.83$	$1.89 \pm 0.12$	$-0.50 \pm 0.08$	$4.24 \pm 0.39$	$-2.07 \pm 0.06$	
	$-6.15 \pm 0.27$	$1.94 \pm 0.13$	$-0.58 \pm 0.04$	$3.89 \pm 0.7$	$-1.23 \pm 0.06$	
	$-6.58 \pm 1.1$	$2.16 \pm 0.13$	$-0.52 \pm 0.18$	$3.56 \pm 2.02$	$-1.18 \pm 0.16$	
GRB050401	$-0.54 \pm 0.05$	$3.35 \pm 0.2$	$-2.10 \pm 0.26$			
	$-0.59 \pm 0.02$	$3.13 \pm 0.31$	$-1.63 \pm 0.05$			
	$-0.64 \pm 0.05$	$2.6 \pm 0.16$	$-1.76 \pm 0.40$			
GRB050408			$-0.56 \pm 0.15$	$5.05^{+1.2}_{-0.5}$	$-1.54 \pm 0.20$	
			$-0.67 \pm 0.09$	$4.48 \pm 1.15$	$-1.35 \pm 0.09$	
			$-0.66 \pm 0.03$	$4.42 \pm 0.08$	$-1.24 \pm 0.19$	
GRB050505			$-0.71 \pm 0.18$	$3.84 \pm 0.46$	$-2.45 \pm 0.40$	
			$-0.79 \pm 0.04$	$3.37 \pm 0.72$	$-2.29 \pm 0.30$	
			$-0.82 \pm 0.16$	$3.40 \pm 0.18$	$-2.29 \pm 0.30$	
Mean Curve	$-2.19 \pm 0.17$	$2.22 \pm 0.31$	$-0.69 \pm 0.07$	$4.91 \pm 0.04$	$-1.99 \pm 0.03$	

(1) Rest frame.

(2) This is a very complex light curve. The slope at the beginning increases with time more or less as for the other light curves. After  $\sim 200$  s it decreases rather slowly and, here is the main anomaly, after  $\sim 800$  s the light curve becomes flat to decrease again after about 8000 s (see Figure 1).

(3) This curve presents a short plateau so that for a small time interval we find almost no slope.

The estimate of the time of the break is the most uncertain quantity. Perhaps the most unbiased procedure to estimate these light curve parameters is: a) fit the observed light curve with any fitting function (a polynomial fit may be the easiest way to do it), b) estimate the slope by the first derivative of the fitting function, and c) estimate the time of the break by measuring the maximum of the curvature. The curvature is given by the following relation where  $f(t)$  is the function fitting the observations:

$$K = \frac{|\partial^2 f(t) / \partial t^2|}{(1 + (\partial f(t) / \partial t)^2)^{3/2}}$$

Although in the third method the estimate of the errors is rather cumbersome, this method does have the advantage of allowing high temporal resolution. On the other hand since all of our estimates agree within the errors we hereafter use results from the first method, which is the simplest approach.

Table 2 shows that the light curves have the fairly common and well known behavior, consisting of a rather fast decay interrupted by light curve breaks.

During the very early phase there are three GRBs which show a steep decay, whereas the light curve of GRB 050401 ( $z=2.9$ ) differs considerably. In this case we note that the early temporal slope is similar to what was observed after the first break in the other three GRBs. Unless we missed an early, fast, and brief decay soon after the BAT prompt phase, this may indicate that we have at least two distinct classes of bursts.

The issue is whether the initial slope of GRB050401, note that this is more or less the same as that observed in the other GRBs after the initial phase, is the beginning of the afterglow or the slope we observe after having missed a steeper decline between 4 s and 30 s (rest frame) that we did not see. We are inclined to disregard this second possibility for the moment because a) we have no evidence from the data at hand to support it, b) by using a definition of the phases anchored to the temporal evolution we better follow the evolution of the facts without biasing with a model and c) a missed initial steeper decline would have meant a flux higher by at least a factor of 10 and therefore detectable by BAT.

The BAT light curve of GRB050319 is characterized by two energy peaks separated by about 137 seconds, the first peak has an equivalent (referred to the XRT band) mean flux of  $5.7 \cdot 10^{-8}$  erg cm $^{-2}$  s $^{-1}$  compared to a flux of  $2.9 \cdot 10^{-8}$  erg cm $^{-2}$  s $^{-1}$  in the second peak. The formal trigger, and therefore our reference of time, is referred to the start of the first peak. By using this time as our reference time, we find the steepest slope for any of the bursts (see Table 4). Conversely, if we use the beginning of the second peak as the trigger time, i.e. 137 seconds after the start of the first peak, the light curve of GRB 050319 becomes almost exactly identical to the light curve of GRB050318. As we will detail later, we are not aware of any plausible physical explanation for decay slopes as steep as -6 or -7 and this may be giving us a clue about the physical trigger time (where by this we mean the real beginning of the afterglow or onset time). This finding highlights the importance of understanding how to observationally measure, or derive, the time at which the afterglow begins.

Indeed, there may exist a strong bias in our analysis since the value of the early slopes are far more strongly dependent upon the choice of  $t_0$ , than slopes determined at later times. Plotting the XRT data with a time beginning at the time of the BAT trigger, as essentially means plotting the function  $L = K (t - t_0)^{-\delta}$  with  $t_0 = t_{\text{trigger}} = 0.0$ . Clearly this has no physical meaning for our purpose since the beginning of the XRT light curve, i.e. the beginning of the afterglow in the current fireball model, quite likely does not coincide with the BAT

trigger, which is simply an operational time. For instance, the big question that is raised by the examination of the rest frame GRB light curves is whether or not the very beginning of the light curve has a constant decay slope and the observed differences are simply due to an incorrect choice of  $t_0$ . Further development of this argument requires detailed simulations of the burst and early afterglow emission and is beyond the scope of the present work. Indeed it is not yet clear whether or not there may be an observation capable of solving or at least clarifying this point.

### GRB\_Rest\_Frame

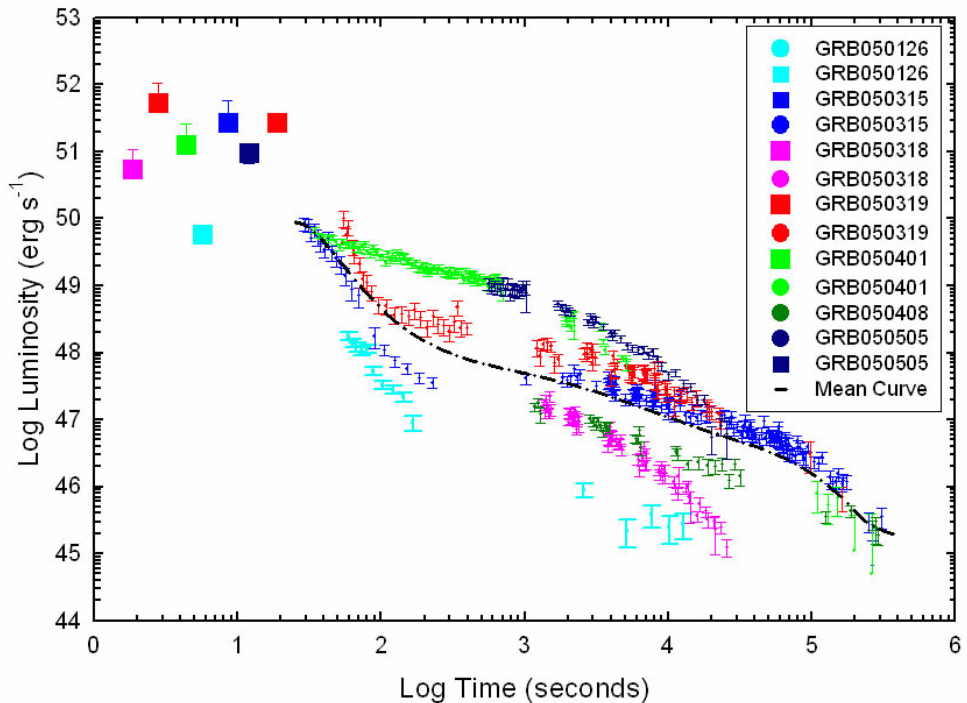


Figure 2: Rest frame light curves for each burst. For the origin of time we used the trigger time as given by the BAT instrument. Squares refer to the mean flux observed by BAT during the burst and converted via the BAT spectrum to the energy band of XRT, circles refers to the observed flux in the band 02 – 10 keV. The dot dashed line is the mean curve as described in the text.

The most striking feature shown by the composite diagram of Figure 2 is a rough decay of the luminosity that proceeds from the BAT to the XRT data with a common trend and a similar coarse slope once we smooth over the details of individual light curves (see Figure 3 for details and the different behavior shown by the light curve of GRB050401 where the afterglow begins with a mild slope  $\delta \approx -0.6$ ). All of the XRT light curves seem to point toward the mean flux observed by BAT (square symbols in Figure 2). This suggests a unique model as a source of the luminosities we observe for the rapid decay class of light curves. For this reason and rather than reporting a simple average of the values measured for each light curve, we have constructed a composite light curve, formed from summing the observations in the rest frame of the sources. The curve is shown in Figure 2 with a dot – dashed line. This exercise is indicative only and should be carried out on a larger sample

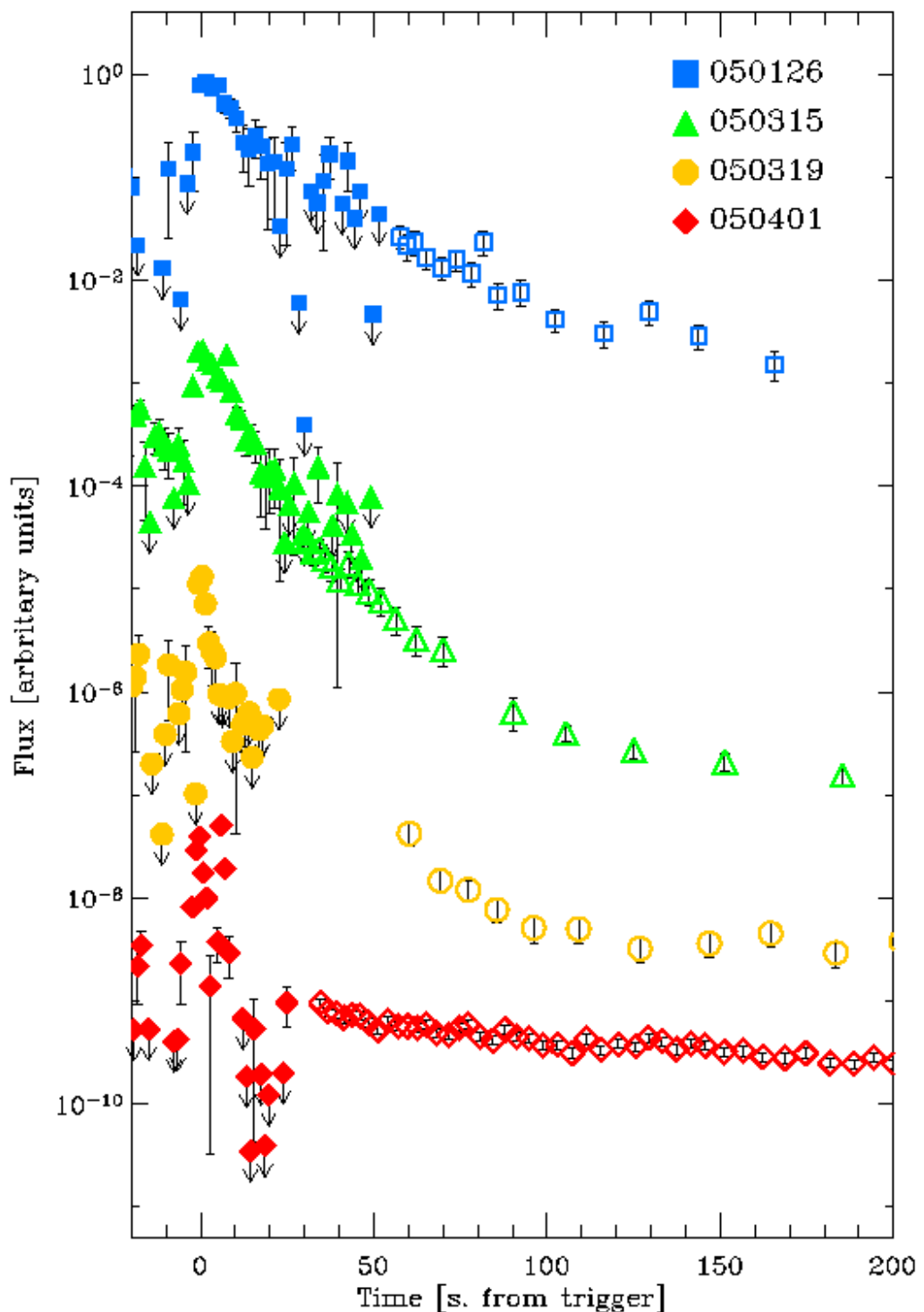


Figure 3. Light curves for 4 of the 7 GRBs observed by Swift for which we have redshift and early XRT observations. In the case of GRB 050315 the BAT and XRT observations overlap.

with well defined GRB subclasses. In particular, the light curve of the GRB 050505 was excluded because it displays rather different characteristics over this time interval, being more similar to the light curve of GRB050401, Figure 2, again suggesting the presence of at least two well-defined classes. Unfortunately, the early phase for GRB050505 could not be observed. Similarly, GRB 050401 was also excluded from our composite decay light curve. Our composite light curve is designed to be representative of a well defined class of objects. We note however that the inclusion of GRB050505 and GRB050401 in the composite light-curve does not alter, however, our conclusions.

To clarify this point, we estimated the energies emitted in soft X-rays (XRT) as a function of the energy emitted in the hard X-rays (BAT). Most of these GRB curves were observed in the range 50 – 200 s (rest frame) and in the range 1300 – 12600 s (rest frame). Therefore we selected these time intervals to characterize the light curves and to estimate the energy emitted during these intervals in soft X-rays. In this way, we do not need to extrapolate or derive a mean curve, and the measurements directly reflect the observations. Integration is in all cases carried out numerically. The results are presented in Table 3. Here we give for each burst (column 1) the spectral index of the prompt emission (column 2) and its absolute fluence (rest frame), column 3. In column 4 and column 5 we report the absolute fluence observed in the XRT band in the time intervals 50 to 200 seconds, and 1300 to 12600 seconds after the BAT trigger. Column 6 gives the XRT absolute fluence during the total duration of the observations, and in column 7 the beginning and the end of the observations (Log seconds) in the rest frame of the source. Note however, that we have gaps due to spacecraft observing constraints.

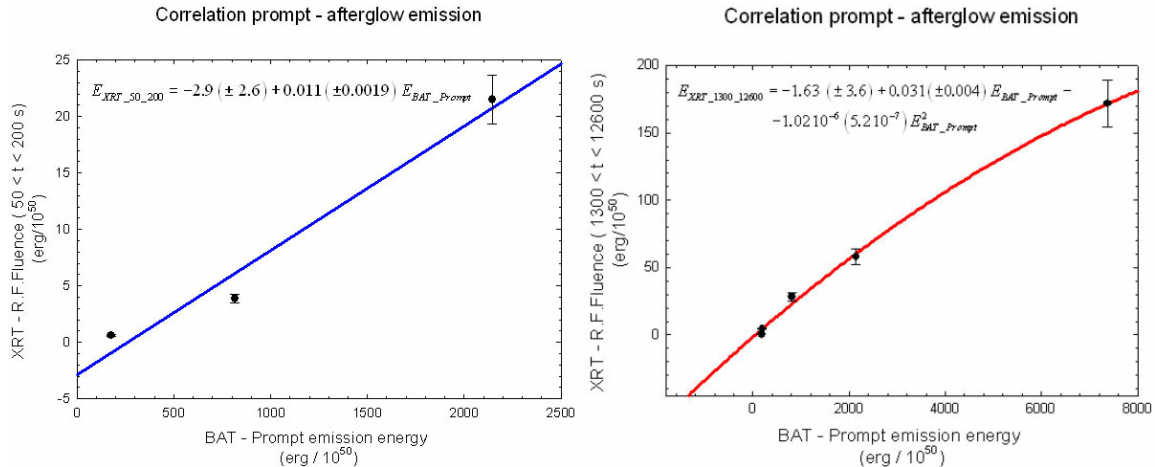


Figure 4. Correlation between the isotropic Energy emitted (in units of  $10^{50}$  erg) during the prompt phase and the isotropic energy emitted in the X-ray band (0.2 – 10 keV) during the afterglow. On the left figure the Energy emitted – Rest Frame Fluence - in the time interval  $50 < t < 200$  s as a function of the prompt emission (as measured by BAT). On the right we show the same correlation for XRT over the time interval  $1300 < t < 12600$  s.

For those bursts for which we observed the XRT light curve soon after the prompt emission (BAT) it is possible to compare the total absolute fluence observed in the soft X-ray with the absolute fluence observed at higher energies, i.e. the ratio of column 6 and 3. The “afterglow” X-ray emission is about 3% of the hard X-ray energy emitted during the

prompt phase except for GRB050315, for which the soft X-rays are about 14% of the prompt emission.

The correlation between the prompt phase and afterglow for these time intervals is plotted in Figure 4. We did not include, however, GRB050401. This burst, as mentioned earlier, behaved differently from all the others. Those with a very sharp decay immediately following the prompt phase, and those with a shallower decay slope, but involving a large amount of energy during the first few hundreds seconds. The larger amount of energy emitted during the first phase by these slow early decay bursts follows directly from their shallower slopes.

We assigned to each measure in figure 4 an error of 10%, as an upper limit. The accuracy of the interpolation of the light curves in the regions 50 – 200 s and 1300 – 12600 respectively and the related integration is much higher so that a 10% error reflects essentially the uncertainty of the flux observations. The probability of obtaining data as different or more different of the fits above is (ANOVA P value) 0.11 for the plot on the left and 0.002 for the plot on the right.

The correlation seems to be very robust albeit for the small sample of bursts. That is the energy in the afterglow is tightly correlated with the energy emitted in the 15 – 350 keV band during the burst. The curvature shown by the second correlation (BAT versus XRT\_1300\_12600) may indicate that at higher energies the response of the Inter Stellar Medium (ISM) saturates, most likely due to a limit on the amount of the shocked matter available.

## 4. Discussion

The fireball model is in very good agreement with the observations of the single bursts as shown by previous observations of GRBs, and more recently by the Swift satellite. On the other hand we need to clarify the detailed evolution of the relativistic jet and understand the time of the beginning of the afterglow. That the internal and external shocks may play a role that differs from burst to burst seems possible, at the same time the fact that the flux of each afterglow is a constant percentage of the flux observed during the prompt phase seems to indicate a rather similar transfer of energy to the ISM. Moreover the trigger time of the afterglow can not differ significantly from the BAT operational trigger time. By investigating the early decline phases, immediately following the prompt emission, we can gain information on the energy balance and ultimately an insight into the mechanism of the internal engine and the nature of the progenitor star(s).

As mentioned previously (Tagliaferri et al. 2005, Burrows et al. 2005b, Cusumano et al. 2005) the fast early decay may be due to either external or internal shocks. Either mechanism may be possible and for a very steep decay, geometrical factors likely dominate. After the shock crossing (heating), the shocked material cools radiatively and adiabatically. Radiation from adiabatically expanding material decays very fast,  $t^{-4.5}$ , and is a strong function of the electron energy distribution. However once the cooling drops below the observed frequency, the flux decays exponentially. In such a case, high latitude emission (off-axis emission) begins to dominate. The expected decay index is  $\alpha = 2 + \beta$ ,  $F_v \propto t^\alpha v^\beta \sim t^{-3}$ . If the decay is steeper than -3 as it may be in the case of GRB050319, we have to appeal to geometric effects, or to a different choice of  $t_0$ .

The second point we make in this work is that, as expected from the preliminary data, we have different classes of GRBs that are characterized by the initial decay. Whether this is due to the environment or to the mechanism of the burst and the progenitor is not yet clear. The light curves with an initial shallow decay may be due to a continuously-fed fireball (Zhang and Meszaros 2001).

The most relevant result is probably the tight, albeit small number statistics, correlation between the prompt energy and the energy emitted by the decaying XRT light curve (Figure 3). Indeed there is an indication that the shock energy may tend to a limit for very energetic bursts so that observations of very energetic bursts, that represent the extreme tail of the distribution, are fundamental in understanding the interaction between the prompt emission and the ISM. Integrating over our mean light curve, which may only be indicative of the most common class of bursts, and which spans a range in time from 30 seconds to about 73 hours after the burst, we derive an emission of about  $9.0 \cdot 10^{51}$  erg. In the interval for which we computed the correlation, that is in the intervals of time 50 – 200 and 1300 – 263027, we have an emission of  $7.8 \cdot 10^{50}$  erg and  $2.0 \cdot 10^{51}$  erg, respectively.

The internal – external shocks model requires a comparable emission of energy during the prompt and the afterglow phases. By contrast, the observations show that the energy in the afterglow is at most 15% of the energy we observe during the prompt phase. Clearly, we require better statistics in order to refine the details of the model and ISM. Indeed, here we are referring only to the energy emitted in the X ray band. We certainly have a broader range of energy related to the prompt phase and it seems likely that the energy transfer to the ISM will be even less. For a theoretical discussion on the relationship, if any, between the prompt and afterglow energy see Lloyd-Ronning & Zhang (2004).

The sharp decrease of the afterglow seems to be correlated with the morphology of the prompt emission as observed by the BAT instrument. The prompt emission is in all cases (GRB050126, GRB050315, GRB050319) characterized by a sharp rise of the light curve and smooth decay. On the contrary for GRB 050401 we have two nearly symmetric peaks, with large fluctuations. The BAT light curve of GRB050319 also shows an earlier (137 seconds) peak that does not show a fast rise. This is another reason why we believe the  $t_0$  of the XRT light curve, which has an exceptionally steep decay using the first trigger, may be more closely related to the second peak. GRB050318 and GRB0500505 were not observed by XRT immediately after the trigger, while for GRB050408 we do not have useful BAT information. The indication therefore is, and this will be clarified with an analysis of a larger sample, that the steep decay of the X-ray curve may correlate with one or other of the prompt peak phases.

The XRT spectra are the best compromise between the temporal resolution of the break timescale and the photon statistics needed to measure spectral parameters. In this small sample we do not have evidence of varying  $N_{\text{H}}$ ; this issue will be treated separately in a much large sample. The main result of the analysis is that the observed energy index shows little, if any, variation among the bursts. For our sample we derive a mean Energy Index =  $1.10 \pm 0.29$ , where the errors of the single derivations as listed in Table 4 range between 0.06 and 0.4. In the case of GRB050319, however, there is a significant variation of the energy index after the first break. The spectrum evolves from very soft (3  $\sigma$  above the mean value) to hard (about 1  $\sigma$  below the mean value) with a total excursion of 4 $\sigma$ . That may be due to new injection of energy from the second burst.

Finally we should stress that knowledge of the combination of the XRT light curve morphology, of the mean values of the related rest frame parameters and the derivation of a mean light curve leads to the estimate of the redshift using the X-ray light curve.

## Acknowledgments

We are grateful to Dino Fugazza who helped us in preparing the manuscript. The work is supported in Italy by funding from ASI on contract number I/R/039/04, at Penn State by NASA contract NAS5-00136 and at the University of Leicester by PPARC contract number PPA/G/S/00524 and PPA/Z/S/2003/00507. We acknowledge in particular all those member of the Swift Team at large who made this mission possible. This goes from the building of the hardware, the writing of the software, the operation at the Mission Operation Centre and the performance of the ASI ground segment at Malindi, Kenya.

## References:

Angelini, L., et al. 2005, GCN 3161  
Barthelmy, S. 2004, SPIE 5165, 175  
Beardmore, A.P., et al. 2005, GCN 3133  
Berger, E., et al. 2005a, GCN 3088  
Berger, E., et al. 2005b, GCN 3122  
Burrows, D.N., Hill, J.E., Chincarini, G., et al. 2005a, Ap.J. 622, L85  
Burrows, D.N., Romano, P., Falcone, A., et al. 2005b, in preparation  
Burrows, D.N., Hill, J.E., Nousek, J.A., et al. 2005c, Adv. Sp. Sc. In press  
Campana, S., Antonelli, A., Chincarini, G., et al. 2005a, Ap.J. 625, L23  
Campana, S., et al. 2005b, GCN 2996  
Chincarini, G., et al. 2005, GCN 3209  
Costa, E., Frontiera, F., Heise, J., et al. 1997, Nature 387, 783  
Cusumano, G., Mangano, V., Angelini, L., et al. 2005, Ap.J. submitted  
Fynbo, J.U., et al. 2005, GCN 3136  
Fynbo, J.U., et al. 2005, GCN 3176  
Gehrels, N., Chincarini, G., Giommi, P., et al. 2004, Ap. J., 611, 1005  
Hill, J.E., Cheruvu, A.F., Abbey, R. M., et al. 2004, SPIE 5165, 217  
Hulliger, D., et al. 2005, GCN3364  
Hurley, K., Sari, R., Djorgovski, S.G. 2002, Astro-ph/0211620  
Lloyd-Ronning & Zhang 2004, ApJ, 613, 477  
Kelson, D., et al. 2005, GCN 3101  
Krimm, H., et al. 2005, GCN 3111  
Krimm, H., et al. 2005, GCN 3117  
Markwardt, C., et al. 2005, GCN 3143  
Meszaros, P. & Rees, M.J. 1993, ApJ 405, 278  
Moretti, A., Campana, S., Tagliaferri, G., et al. 2004, SPIE 5165, 232  
Parsons, A., et al. 2005, GCN 3094  
Piran, T. 1999, Physics Reports, Volume 314, Issue 6, p. 575-667.  
Prochaska, J.X., et al. 2005, GCN 3204

Sakamoto, T., et al. 2005, GCN 3189

Sato, G., et al. 2005, GCN 2987

Tagliaferri, G., Goad, M., Chincarini, G., et al. 2005, *Nature*, in prep.

Zhang & Meszaros 2001, *ApJ*, 552, L35

Zhang, B. and Meszaros, P. 2004, *IJMPA*, 15, 2385